PRP Pharmacology Research & Perspectives
Open Access

ORIGINAL ARTICLE

Preclinical evaluation of SMM-189, a cannabinoid receptor 2-specific inverse agonist

Chaela Presley, Ammaar Abidi, Satyendra Suryawanshi, Suni Mustafa, Bernd Meibohm & Bob M. Moore II

Department of Pharmaceutical Sciences, College of Pharmacy, University of Tennessee Health Science Center, Memphis, Tennessee

Keywords
ACTOne, cannabinoid receptor 2, inverse agonist, microglia, polarization

Correspondence
Bob M. Moore, 847 Monroe Ave. Ste 327, Memphis, TN 38163. Tel: (901) 448-6085; Fax: 901-448-6828; E-mail: bmoore@uthsc.edu

Funding Information
The University of Tennessee Health Science Center (UTHSC), College of Pharmacy, and the UTHSC Neuroscience Institute provided the stipend for Chaela Presley. Endece LLC provided funding for the ACTOne assay and the biopharmaceutical evaluation of SMM-189. This work was also funded in part by National Institutes of Health grant 1S10OD016226 (Meibohm).

Received: 24 March 2015; Revised: 27 May 2015; Accepted: 31 May 2015

Pharma Res Per, 3(4), 2015, e00159, doi: 10.1002/prp2.159

doi: 10.1002/prp2.159

Abstract

Cannabinoid receptor 2 agonists and inverse agonists are emerging as new therapeutic options for a spectrum of autoimmune-related disease. Of particular interest, is the ability of CB2 ligands to regulate microglia function in neurodegenerative diseases and traumatic brain injury. We have previously reported the receptor affinity of 3′,5′-dichloro-2,6-dihydroxy-biphenyl-4-yl)-phenyl-methanone (SMM-189) and the characterization of the beneficial effects of SMM-189 in the mouse model of mild traumatic brain injury. Herein, we report the further characterization of SMM-189 as a potent and selective CB2 inverse agonist, which acts as a noncompetitive inhibitor of CP 55,940. The ability of SMM-189 to regulate microglial activation, in terms of chemokine expression and cell morphology, has been determined. Finally, we have determined that SMM-189 possesses acceptable biopharmaceutical properties indicating that the triaryl class of CB2 inverse agonists are viable compounds for continued preclinical development for the treatment of neurodegenerative disorders and traumatic brain injury.

Abbreviations

CB1, cannabinoid receptor 1; CB2, cannabinoid receptor 2; CD16/32, Fc γII/III receptor; CD206, mannose receptor; CP 55,940, 2-[(1R,2R,5R)-5-hydroxy-2-(3-hydroxypropyl) cyclohexyl]-5-(2-methyloctan-2-yl)phenol; HEK-CNG+CB1, human embryonic kidney cells transfected with a cyclic nucleotide-gated channel and cannabinoid receptor 1; HEK-CNG+CB2, human embryonic kidney cells transfected with a cyclic nucleotide-gated channel and cannabinoid receptor 2; HEK-CNG, human embryonic kidney cells transfected with a cyclic nucleotide-gated channel; IP-10, CXCL10 or Interferon gamma-induced protein 10; KM-233, (−)-(6a*R*,7,10,10a*R*)-tetrahydro-6,6,9-trimethyl-3-(1-methyl-1-phenylethyl)-6H dibenzo [b,d]pyran-1-ol; LC-MS/MS, liquid chromatography–mass spectroscopy/mass spectroscopy; MCP-1, CCL2 or monocyte chemotactic protein 1; MIP-1β, CCL4 or Macrophage inflammatory protein-1β; mTBI, mild traumatic brain injury; PHMG, primary human microglia; PTx, pertussis toxin; SMM-189, 3′,5′-dichloro-2,6-dihydroxy-biphenyl-4-yl)-phenyl-methanone; TARC, CCL17 or thymus and activation-regulated chemokine.

Introduction

The endocannabinoid system and the cannabinoid receptors 1 and 2 (CB1 and CB2) have emerged as important targets for the regulation of inflammation and immune function (Shohami et al. 2011; Crowe et al. 2014; Witkamp and Meijerink 2014). While both receptors are reported to affect inflammatory and immune responses, the CB2 receptor holds significant potential due to the widespread distribution in immune cells and the lack of psychotropic effects associated with the CB1 receptor. In a spectrum of diseases, ranging from autoimmune to

neurodegenerative disorders, the CB2 receptor has been identified as a potential target for the development of new chemotherapeutic interventions (Croxford 2003; Sipe et al. 2005; Lou et al. 2011).

Regulation of CB2 function is particularly attractive in neuroinflammation and neurodegenerative diseases since activated microglia are reported to upregulate the expression of CB2 (Ashton and Glass 2007; Stella 2010). This observation appears to be specific to the diseased brain thus providing a unique target for drug intervention. Specifically, microglia protect and repair the damaged brain. However, chronic activation can result in sustained release of proinflammatory cytokines and chemokines, enhanced microglia migration, as well as recruitment of peripheral monocytes and T cells, thus exacerbating the primary CNS damage (for excellent reviews see (Block et al. 2007; Friese and Fugger 2007; Ebner et al. 2013)). CB2 ligands may be beneficial in mitigating the adverse outcomes of chronic activation by inhibiting the release of proinflammatory cytokines and chemokines in addition to regulating microglia migration (Walter et al. 2003; Ortega-Gutierrez et al. 2005; Lunn et al. 2008; Romero-Sandoval et al. 2009; Fraga et al. 2011; Louvet et al. 2011; Martin-Moreno et al. 2011; Zarruk et al. 2012). However, the required functional activity of CB2 ligands, that is, agonist, neutral antagonist, or inverse agonist, to effectively regulate chronic activation remains an open question. This is exemplified by studies reporting both CB2 agonists such as JWH 015 and CB2 inverse agonists SR 144528 and AM 630 induce anti-inflammatory changes in microglia (Ribeiro et al. 2013). To further complicate the CB2 functional requirement, it is also reported that activity of compounds such as cannabidiol and Δ^9-THC is independent of CB2 when inverse agonist SR 144528 is employed to block their CB2 agonist activity (Kozela et al. 2010).

The mechanisms whereby CB2 modulation affects inflammation and immune cell function are complex and detailed pathways remain to be determined (Bouaboula et al. 1996; Mukhopadhyay et al. 2006; Merighi et al. 2012). Notwithstanding, CB2 agonists and inverse agonists have demonstrated significant potential in immunomodulation (Rhee and Kim 2002; Elliott et al. 2011; Ribeiro et al. 2013; Zoppi et al. 2014; Reiner et al. 2015). This provides the impetus for the development of new chemical entities to regulate inflammatory responses, regulate immune cell activity, and provide probes for studying signaling pathways associated with CB2 ligation. We previously reported the synthesis and preliminary characterization of 3′,5′-dichloro-2,6-dihydroxy-biphenyl-4-yl)-phenyl-methanone (SMM-189) and demonstrated the preferential binding to the CB2 receptor (Bhattacharjee et al. 2009). Furthermore, we have evaluated the efficacy of SMM-189 in a murine model of mild traumatic brain injury (mTBI). In these studies, SMM-189 improved motor, visual, behavioral deficits, and mitigated eye and axonal damage associated with mTBI (Reiner et al. 2015). These results prompted us to conduct a detailed evaluation of the functional activity of SMM-189, the efficacy in regulating microglia function, and the in vitro and in vivo biopharmaceutical properties reported herein.

Materials and Methods

Reagents

G418 was purchased from KSE Scientific (Durham, NC). Puromycin, DMEM, penicillin/streptomycin, gentamicin, DPBS, Hank's Buffer, HEPES, EDTA, Tris base, sucrose, $MgCl_2$, Millipore filter plates and punch kits, EcoLite scintillation cocktail, and Poly-D-lysine coated 96-well plates were purchased from Fisher Scientific (Waltham, MA). Ambisome and FBS were purchased from Atlanta Biologicals (Flowery Branch, GA). Ro 20-1724, acetonitrile, DMSO, lipopolysaccharide (LPS), polyethyleneamine, and fatty acid-free BSA were purchased from Sigma Aldrich (St. Louis, MO). Antibodies against murine CD16/32 (ab33550) and CD206 (ab64693) were purchased from Abcam (Cambridge, UK). High bind plates (L15XB-3), anti-rat (R32AA-5), and anti-rabbit (R32AB-1) SULFO-TAG antibodies were purchased from Meso-Scale Discovery (Gaithersburg, MD). Cellular dyes phalloidin and Hoechst were purchased from Cellomics (Pittsburgh, PA), and ACTOne Membrane Potential Dye was purchased from Codex BioSolutions (Gaithersburg, MD). Forskolin, CP 55,940, HU 308, JWH 133, and SR 144528 were purchased from Tocris (Bristol, UK). Tritiated CP 55,940 was purchased from PerkinElmer (Waltham, MA). The 96-well filter plates and punch tips were purchased from Millipore (Billerica, MA).

Cell culture

The HEK-CNG parental cell line, HEK-CNG+CB1, and HEK-CNG+CB2 cell lines were purchased from Codex BioSolutions, Inc (Gaithersburg, MD). HEK-CNG cells were cultured in DMEM with 10% FBS, 1% P/S, and 25 μg/mL G418 at 37°C, 5% CO_2. HEK-CNG+CB1 and HEK-CNG+CB2 cells were cultured in DMEM with 10% FBS, 1% P/S, 25 μg/mL G418, and 5 μg/mL puromycin. Cells were passaged every 2–3 days or when confluence reached 80%. C8B4 murine microglia of unknown sex were purchased from ATCC (Manassas, VA) and cultured in DMEM with 10% FBS and 1% P/S according to the manufacturer's directions. Primary human microglia of unknown sex (PHMG) were purchased from Clonexpress, Inc (Gaithersburg, MD). These cells were certified to be

free of HIV, hepatitis B and C, bacteria, fungi, and mycoplasma. PHMG were thawed rapidly at 37°C, added to 5 mL of DMEM:F12 50:50 with 25 μg/mL gentamicin, 2.5 μg/mL ambisome, 1% P/S, and 5% FBS, and centrifuged at 125*g* for 5 min. Cells were counted and immediately plated at a density of 30,000 cells/100 μL.

Membrane preparations

HEK-CNG+CB1 or HEK-CNG+CB2 cells were plated in 500 cm^2 culture dishes and grown in 100 mL selection medium to 80% confluence. After removing medium, cells were washed gently with 10 mL of ice cold PBS. Then 10 mL of ice cold PBS with 10 mmol/L EDTA was added, and cells were scraped. The resulting cell suspension was centrifuged at 4°C, 500*g* for 5 min. The supernatant was then discarded and the pellet homogenized in 10 mL of ice cold 50 mmol/L Tris-HCl, 320 mmol/L sucrose, 2 mmol/L EDTA, 5 mmol/L $MgCl_2$ at pH 7.4 (solution A). The cell suspension was centrifuged at 4°C, 1600*g* for 10 min. The supernatant was saved, and the cell pellet washed three times in 8 mL of solution A, each time homogenized for 10 min and centrifuged at 4°C, 1600*g* for 10 min. Each time the supernatant was saved and combined with the previously saved supernatant. The combined supernatant was centrifuged at 4°C, 50,228*g* for 3 h. The supernatant was then discarded and the pellet suspended in 3 mL of 50 mmol/L Tris-HCl, 2.5 mmol/L EDTA, 5 mmol/L $MgCl_2$, 10% (w/v) sucrose at pH 7.4 (solution B). Protein concentration was evaluated using a Pierce BCA protein assay kit. Membrane aliquots were stored at −80°C. Scatchard analysis on membrane preparations was done by varying [^{3}H]-CP 55,940 final concentrations from 10 pmol/L to 10 nmol/L both with and without 10 μmol/L WIN 55,212-2 to determine nonspecific binding. CB1 membrane preparation K_d was 2.55 nmol/L and B_{max} was 1 pmol/mg. CB2 membrane prepration K_d was 2.0 nmol/L with B_{max} 2 pmol/mg. Binding buffer was made as follows: 50 mmol/L Tris–HCl, 5 mmol/L $MgCl_2$, 2.5 mmol/L EDTA, 0.5 mg/mL fatty acid-free bovine serum albumin, pH 7.4.

Note: The K_is for SMM-189 differs in this report from our previous assay. We have compared the previous and current assay conditions and determined the following: (1) the K_d between the purchased preparations (PerkinElmer Life Sciences) and the ACTOne membranes differ significantly 0.12 versus 2.0 nmol/L, respectively; (2) the [^{3}H]-CP 55,940 used previously was approximately 2.5 years old. To examine differences in preparations potentially affected the affinities, we conducted binding assays on the previously reported compounds (4, 5, 6, and 7, Bhattacharjee et al.) under the current conditions then back calculated the EC_{50}s using the Cheng–Prusoff equation (Table S1). The first observation is that there is no correlation between the EC_{50}s for CB2 for the individual preparations suggesting that the purchased preparations may have been improperly stored. Alternatively or in combination decomposition of the radioligand is a potential source of deviation. It is reported that the rate of decomposition is initially 3% for 3 months thereafter it is not linear. To our knowledge, there is no information on the identity of the decomposition products. It is plausible that a degradation product could exhibit higher CB1 and lower CB2 affinities resulting in lower and higher affinities, respectively, for our compounds. Unfortunately, the original membrane preparation and [^{3}H]-CP 55,940 are unavailable and as such a definitive explanation of the disparities is not possible.

Receptor binding

Filter plates were filled with 210 μL/well of 0.05% (w/v) polyethyleneamine in deionized water and incubated for 1 h at room temperature. Plates were then filtered using a vacuum manifold and washed five more times with 250 μL/well of deionized water prior to assay. Each well contained 125 μL binding buffer, 5 μL of [^{3}H]-CP 55,940 (final concentration 1–2 nmol/L), 10 μg (in 20 μL) of membrane protein homogenized in binding buffer, and 50 μL SMM-189 in binding buffer at final concentrations ranging from 1 nmol/L to 10 μmol/L. Plates were incubated at 30°C for 90 min. After incubation, membrane solutions were removed via vacuum and washed nine times with 250 μL/well of binding buffer. The filter plate backing was then removed, vacuumed dry, and individual filters punched out using punch tips, into 5 mL of Ecolite scintillation cocktail in 7-mL scintillation vials. Vials were left overnight and read the next day on PerkinElmer Liquid Scintillation Analyzer Tri-Carb 2810TR using a 3-min dwell time. All binding studies were carried out with a minimum of six biological replicates.

ACTOne assay

In order to determine functional pharmacology of the tested compound, HEK-CNG, HEK-CNG+CB1, and HEK-CNG+CB2 cells were plated at 50,000 cells/100 μL medium in clear Poly-D-lysine coated 96-well plates in DMEM 10% FBS, 1% P/S medium the day before experiments were performed. For pertussis inhibition experiments, HEK-CNG+CB2 cells were incubated overnight with 4 ng/mL of pertussis toxin (PTx) prior to experimentation. The day of the experiment, ACTOne formulation Membrane Potential Dye was warmed to 37°C and 100 μL added to each well, followed by 1 h incubation in the dark at room temperature. SMM-189 was tested at

final concentrations from 5×10^{-6} to 5×10^{-10} with 25 μmol/L Ro 20-1724, and 800 nmol/L forskolin in DPBS with 2.5% (v/v) DMSO. Once SMM-189 or CP 55,940, Ro, forskolin, and buffer were added, plates were read using a BioTek (Winooski, VT) plate reader (Ex 540 nm, Em 590 nm) at 50 min. At least six biological replicates were used for subsequent data analysis.

In order to determine antagonist pharmacology, 30 min after adding cation-sensitive dye, 20 μL of SMM-189 in DPBS with 2.5% DMSO was added to each well and incubated for an additional 30 min in the dark at room temperature prior to addition of CP 55,940. Concentrations of SMM-189 were chosen to span concentrations roughly one log above and below the previously determined EC_{50}. To initiate antagonist studies, 30 μL of CP 55,940 made in DPBS with 2.5% DMSO buffer, Ro 20-1724 (final concentration 25 μmol/L), and forskolin (final concentration 800 nmol/L) was added to each well, and the plate was read at 50 min. Six independent experiments were used for subsequent data analysis.

On cell polarization assay

C8B4 microglia were plated at a density of 20,000 cells/50 μL of DMEM with 10% FBS and 1% P/S on High bind plates (Meso-Scale Discovery, Gaithersburg, MD). The next day, 10% FBS containing medium was gently removed and replaced with 100 μL DMEM with 1% FBS and 1% P/S. The third day, 100 μL of DMEM with 1% FBS and 1% P/S containing 2 μg/mL of LPS (final well concentration was 1 μg/mL LPS) was added to each well. One hour later, CB2 ligands (HU 308, JWH 133, SR 144528, or SMM-189) were added in 50 μL containing 5X previously determined EC_{50} and 1X LPS. After 24 h, medium was discarded, and 2 μg/mL of CD16/32 or CD206 antibodies were added in 30 μL PBS to each well for a 2-h incubation followed by a gentle 150 μL PBS wash. Then, 30 μL of either 2 μg/mL anti-rat (CD16/32) or anti-rabbit (CD206) SULFO-TAG antibody was added for another 2-h incubation. After three gentle washes with 150 μL/well, 150 μL of 2X surfactant free read buffer was added and the plate was read on a SECTOR 2400 Imager (Meso-Scale Discovery, Gaithersburg, MD). Data were normalized to LPS control and analyzed via ANOVA in GraphPad Prism 6.0 (La Jolla, CA).

Chemokine measurement

Secreted levels chemokines were assessed after treating 30,000 PHMG/well with 1 μg/mL LPS for 0, 12, and 24 h. SMM-189 was added at a previously determined EC_{50} of 9.8 μmol/L 1 h after addition of LPS. After the specified time of incubation, Ultrasensitive Chemokine Plates (MesoScale Discovery, Gaithersburg, MD) were used to assay the concentration of chemokines secreted in medium. Plates were processed according to the manufacturer's instructions and then imaged using the Sector 2400 Imager. Protein quantification was done using the MesoScale Discovery software (Gaithersburg, MD). Each group had four biological replicates.

Cell staining and microscopy

Microglia were treated as described in the Chemokine measurement section, but after 0, 12, or 24 h in were stained using phalloidin to mark actin and Hoechst to mark nuclei. Cells were imaged using a Zeiss LSM710 (Jena, Germany) laser scanning confocal microscope, using the 405 nm laser line for Hoechst and the 561 nm laser line for phalloidin. To quantify morphology, a series of images from four fields for each treatment group at 24 h were blinded and given to four investigators not associated with these studies with instructions to count spherical versus rod-like morphology. Note: Since the time course studies were conducted on single plates, reverse addition method was applied for the drug treatment, that is, 24 h back to 0 h such that all samples were fixed simultaneously, to prevent potential complicating effects of paraformaldehyde from adjacent wells.

Physiochemical property assessment

cLogP was estimated using ChemDraw Ultra 10.0. Solubility was determined at pH 7.4 using a miniaturized shake-flask method (Glomme et al. 2005). Drug suspension was shaken for 24 h in a buffer solution at room temperature, centrifuged and the supernatant analyzed by LC-MS/MS. Permeability was determined by a parallel artificial membrane permeability assay (PAMPA) in 96-well format at pH 7.4 as previously described (Kerns et al. 2004). Permeability was measured after 18-h incubation via UV absorbance in a microplate reader (DTX880, Beckman Coulter).

Liver microsome metabolism

The in vitro stability of SMM-189 was assessed in pooled rat liver microsomal preparations (BD Biosciences, Franklin Lakes, NJ) by monitoring disappearance of the compound over an incubation period of 90 min. The percentage of intact parent compound was estimated using the LC-MS/MS assay.

Plasma protein binding

Protein binding was determined at biologically relevant concentrations of SMM-189 (500 ng/mL and 2 μg/mL) in

rat plasma with the RED® equilibrium dialysis device at 37°C (Pierce Biotechnology Inc., Rockford, IL). Aliquots of plasma and the isotonic phosphate buffer, pH 7.4 in the receiving compartment were analyzed for SMM-189 concentrations by LC-MS/MS, and the free fraction was calculated as ratio of the concentrations in the buffer and the initial concentration in plasma.

Pharmacokinetic studies

Animal studies were performed under a University of Tennessee Health Science Center Institutional Animal Care and Use Committee approved protocol. Male Sprague–Dawley rats (Harlan Labs, Indianapolis, IN) ($N = 6$; approx. 250 g weight) that were catheterized in the external jugular vein and femoral vein received a single intravenous dose of 5 mg/kg SMM-189 formulated in 5% (v/v) 200 proof ethanol, 5% (v/v) Cremophor ELP, and 90% normal saline. Blood samples (200–300 μL) were drawn from the jugular vein catheter pre-dose and 0.17, 0.33, 0.5, 1, 1.5, 2, 4, 6, 8, and 12 h after the dose, and were immediately centrifuged at 2000*g*, 4°C for 10 min. Plasma fractions were harvested and stored at −70°C until analysis by LC-MS/MS.

Quantification of compound concentrations by LC-MS/MS

A total of 50 μL aliquots of plasma were prepared by protein precipitation with 200 μL methanol (spiked with the internal standard KM-233, structure 2 in reference (Krishnamurthy et al. 2008)) followed by centrifugation at 10,000*g* for 10 min at 4°C. Chromatographic separation of the supernatant was carried out on a Gemini 5 μm C18 150 × 4.6 mm column (Phenomenex, Torrance, CA) using a mobile phase of acetonitrile and water (75:25, % v/v) at a flow rate of 0.3 mL/min in isocratic mode. Detection was performed with an API 3000 triple-quadruple mass spectrometer (ABI-Sciex, Foster City, CA) with electrospray ionization in multiple reaction monitoring mode using the compound-specific mass transfers of m/z 357→185 for SMM-189, and m/z 377→334 for KM-233. A calibration curve ranging from 0.95 to 5000 μg/L was constructed and validated with spiked samples of rat plasma. The peak area ratios of analyte to the internal standard were linear over the tested concentration range, with a correlation coefficient >0.998. Accuracy (deviation of the analyzed quality control samples from nominal values) was within ±4.2% over the entire range of the calibration curve, and the precision (coefficient of variation of repeated measurements of the quality-control samples) was ≤7.1%.

Data analysis

Scatchard experiments were evaluated with one site-binding hyperbola analysis in GraphPad Prism 6.0. Receptor-binding calculation was also done using a one site-binding model with fixed radionuclide addition and Kd. Raw fluorescence readings from the ACTOne assay were normalized using a feature scaling equation:

$$X' = A + \frac{(X - X_{\min})(B - A)}{X_{\max} - X_{\min}},$$

where forskolin stimulation is the experimental maximum B, blank well with dye and cells only is the experimental minimum A, normalized value is X', $X_{\max}$ is 100%, and $X_{\min}$ is 0%. Data were then analyzed using nonlinear regression analysis. Antagonist studies raw fluorescence readings were normalized with reference to the maximal inhibitory of effect of CP 55,940 as A, minimal inhibitory effect as B, $X_{\max}$ as 100%, and $X_{\min}$ as 0%. Normalized fluorescence values and EC_{50} values were compared to baseline values using Student's *t*-test. Chemokines were analyzed for statistical significance using ANOVA. All statistical evaluations were done in GraphPad Prism 6.0 (La Jolla, CA). Pharmacokinetic parameters were determined from the measured plasma concentration profiles by standard noncompartmental analysis using the software package Phoenix WinNonlin 6.3 (Icon Development Solutions, Hanover, MD) (Gibaldi and Perrier 1982).

Results

Pharmacologic properties of SMM-189

The K_i for SMM-189 (Fig. 1) was lower at the CB2 receptor with a value of 121.3 nmol/L compared to that found at the CB1 receptor 4778 nmol/L—a CB1/CB2 ratio of 39.4, demonstrating a modest selectivity of SMM-189 for the CB2 receptor (Table 1). The functional activity of SMM-189 was evaluated using the ACTOne cell-based cAMP assay in HEK-CNG+CB1, HEK-CNG+CB2, and parental HEK-CNG cells. In the HEK-CNG+CB2 cell system, SMM-189 caused a dose-dependent increase in cAMP-driven fluorescence (~55% over baseline) thus demonstrating the inverse agonist functional activity at CB2 (Fig. 2A). Overnight treatment of the HEK-CNG+CB2 cells with pertussis toxin abolished the aforementioned inverse agonist activity (Fig. 2C). This indicates that, in the ACTOne cell-based assay, CB2 manifests significant constitutive activity and the inactive state of CB2 bound by SMM-189 may sequester $G_{i/o}$ resulting in increased adenylate cyclase activity. Treatment of the

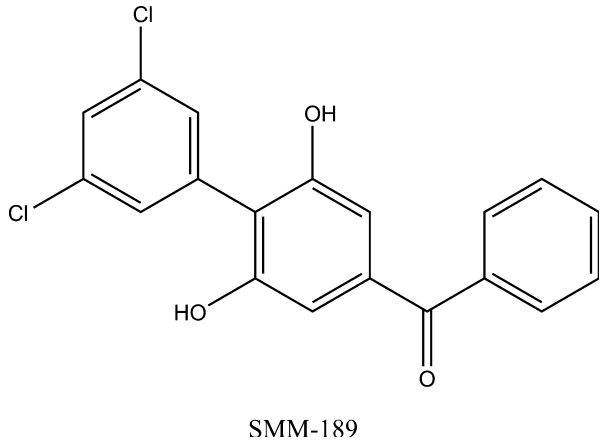

SMM-189

Figure 1. Structure of 3′,5′-dichloro-2,6-dihydroxy-biphenyl-4-yl)-phenyl-methanone.

Table 1. Pharmacologic properties of SMM-189.

	CB_1	CB_2
Receptor binding K_i (nmol/L)	4778 ± 246	121.3 ± 20.6
Functional EC_{50} (nmol/L)	–	153.4 ± 22.25
Maximum response (%)	NS	54.8 ± 3.23

SMM-189, 3′,5′-dichloro-2,6-dihydroxy-biphenyl-4-yl)-phenyl-methanone

HEK-CNG+CB1 with increasing concentrations of SMM-189 resulted in an elevation in cAMP-driven fluorescence that was not significantly different from parental HEK-CNG cells (Fig. 2B). In parental HEK-CNG cells, there was no change in cAMP-driven fluorescence (Fig. 2D) thus SMM-189 selectively increases cAMP via CB2.

The functional activity of SMM-189 was further studied by assessing its antagonistic effects on agonist-driven decreases in cAMP fluorescence production. The nonselective CB1 and CB2 agonist CP 55,940 were selected as our control compound (Govaerts et al. 2004). In the HEK-CNG+CB1 and HEK-CNG+CB2, the control CP 55,940 demonstrated an average 90 percent reduction in cAMP response, whereas no response was observed using the parental HEK-CNG cells. Competition studies using SMM-189 against CP 55,940 in HEK-CNG+CB1 cells showed that SMM-189 has no significant effect in shifting cAMP response curves (Fig. 3A), which is consistent with its very weak receptor binding and lack of CB1 receptor functional activity.

Conversely, in the HEK-CNG+CB2 cells, SMM-189 at low concentrations of CP 55,940 demonstrated the ability to elevate cAMP levels above basal levels, which is consistent with that of noncompetitive antagonists (Fig. 3B). This upward shift of cAMP accumulation was significant at an SMM-189 concentration of 110 nmol/L ($P < 0.01$), a value close to the EC_{50}. At high concentrations of SMM-189, cAMP levels were significantly elevated above CP 55,940 suppression of cAMP, but only at SMM-189 concentrations of 4500 nmol/L and 11000 nmol/L (11 μmol/L). The EC_{50}s of CP 55,940 curves shifted significantly to the right for all tested concentrations of SMM-189 except 110 nmol/L, with correspondingly higher significance at higher concentrations.

On cell polarization assay

In order to determine the effects of selective CB2 agonists (HU 308 and JWH 133) and inverse agonist (SMM-189 and SR 144528) on activated microglia, we stimulated C8B4 murine microglia with LPS. One hour following LPS stimulation, CB2 ligands were added at respective EC_{50}s and after 24 h incubation were evaluated for polarization markers to either: (1) CD16/32 which is a marker of a proinflammatory state consistent with LPS activation (often referred to as M1) or (2) CD206 which is a marker of a pro-wound healing state consistent with alternative activation (often referred to as M2). CB2 agonists HU 308 and JWH 133 decreased CD16/32 expression compared to LPS controls, although only HU 308 did so significantly ($P < 0.001$) and was significantly better at decreasing CD16/32 than JWH 133 ($P < 0.0001$) (Fig. 4A). CB2 inverse agonists SR 144528 and SMM-189 also decreased CD16/32 expression in comparison to LPS control, but only SMM-189 did so significantly ($P < 0.001$) and decreased CD16/32 significantly more than did SR 144528 ($P < 0.05$).

The M2 response of microglia to the presence of agonist and inverse agonist was surprising. CB2 agonists HU 308 and JWH 133 significantly decreased CD206 ($P < 0.001$, $P < 0.01$). A comparison of the two agonists revealed that HU 308 treatment resulted in a significantly lower level of CD206 compared to JWH 133 treatment ($P < 0.0001$) (Fig. 4B). CB2 inverse agonists exhibited the opposite effect wherein pro-wound healing markers increased relative to LPS control cells. SR 144528 and SMM-189 both significantly increased CD206 ($P < 0.001$, $P < 0.01$) and were not significantly different from each other (NS). The results from this study are consistent with the alteration in chemokine profiles and the morphological changes associated with SMM-189 treatment of LPS-stimulated microglia (see below).

Effect of SMM-189 on activated PHMG secretion of chemokines

To evaluate the effect of SMM-189 on activated microglia, and the potential role of the compound in

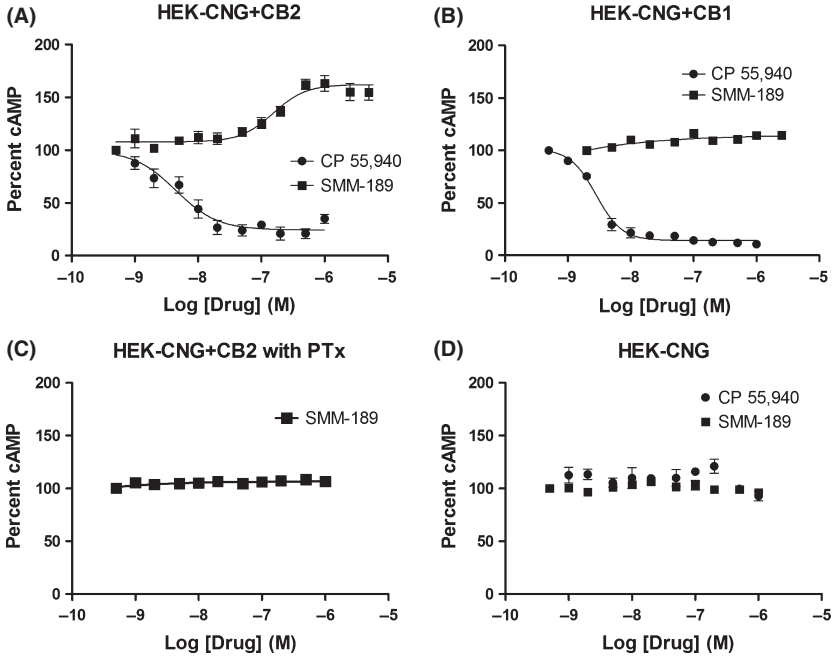

Figure 2. Pharmacologic assessment of SMM-189 using the ACTOne assay. (A) SMM-189 increases cAMP in HEK-CNG+CB2 cells, (B) SMM-189 does not change cAMP levels in HEK-CNG+CB1 cells, (C) SMM-189 elicits no change in cAMP in HEK-CNG+CB2 treated overnight with pertussis toxin (PTx), (D) SMM-189 had no effect on cAMP levels in parental HEK-CNG cells. $N = 6–14$, error bars ±SEM. HEK-CNG+CB1, Human embryonic kidney cells transfected with a cyclic nucleotide-gated channel and cannabinoid receptor 1; SMM-189, 3′,5′-dichloro-2,6-dihydroxy-biphenyl-4-yl)-phenyl-methanone.

neuroinflammation (Liu and Hong 2003), we stimulated PHMG with LPS. The study was designed to control for the potential effects of media addition on this reactive cell type, thus a media addition and media + SMM-189 were designed into the study. A comparison of media and media + SMM-189 revealed no significant difference in chemokine expression (Fig. 5). At the 12-h time interval, LPS-stimulated PHMG expressed statistically significantly higher levels of eotaxin, eotaxain-3, IP-10, TARC, and MIP-1β, and after 24 h MCP-1 was also significantly increased, compared to media and media + SMM-189 controls ($P < 0.01–0.001$) (Fig. 5). SMM-189 treatment 1 h after LPS stimulation decreased eotaxin secretion significantly at 24 h (Fig. 5A). Eotaxin 3 levels for LPS + SMM-189 were not significantly different from the LPS alone group at either time point (Fig. 5B). The levels of IP-10 decreased significantly in response to LPS + SMM-189 treatment at 12 ($P < 0.05$) and 24 h ($P < 0.0001$) (Fig. 5C). There was no significant difference in MCP-1 expression until 24 h postdrug treatment after which a significant decrease in MCP-1 was observed combining SMM-189 with LPS ($P < 0.05$) (Fig. 5D). TARC expression after LPS treatment was significantly decreased following SMM-189 treatment but still significantly higher than media controls at both 12 and 24 h (Fig. 5E). MIP-1β expression was unaffected by SMM-189 treatment at 12 h, but was significantly decreased in comparison to LPS alone groups at 24 h ($P < 0.01$) (Fig. 5F).

Morphological changes in PHMG in the presence and absence of LPS and SMM-189

We further studied the effects of SMM-189 on normal and activated PHMG via confocal microscopy to determine if unique morphologies associated with different activation states of microglia were manifest. At time 0, all treatment groups exhibited a spherical morphology with some projections present (Fig. 6). This is consistent with other reports suggesting an unstimulated microglial state (Lively and Schlichter 2013). After 12 h, media controls exhibited a contraction in size with the emergence of projections from the cell body. In media + SMM-189 group, a mixture of morphologies including spherical and cell body projections are present with notable emergence of rod-shaped PHMG. A similar shape distribution was also observed in the LPS + SMM-189 treated PHMG. In contrast, the LPS-treated cells were predominately enlarged amoeboid or significantly contracted with relatively few cell body projections. The difference in treatment groups was very pronounced at 24 h with the media control PHMG contracting and extending numerous projections from the cell body consistent with unstimulated microglia.

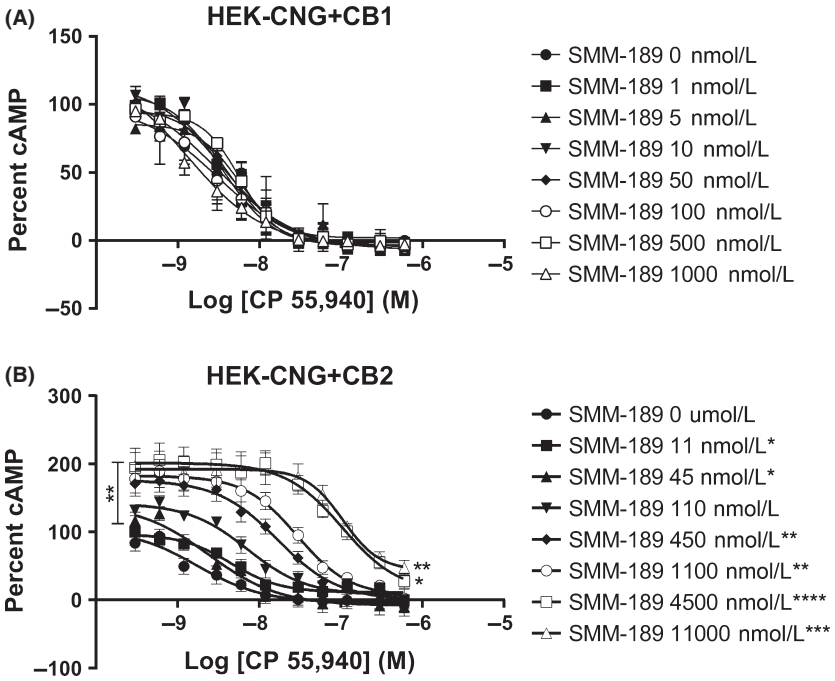

Figure 3. (A) In HEK-CNG+CB1 cells, SMM-189 has no effect on CP 55,940 activity. (B) In HEK-CNG+CB2 cells, SMM-189 increases maximum cAMP activity even in the presence of CP 55,940. $N = 7$, error bars ±SEM. Asterisks at the lowest tested concentration of CP 55,940 represent a significant SMM-189-driven increase in cAMP levels above basal levels, $^{**}P < 0.01$ (*t*-test with basal). Asterisks at the highest tested concentration of CP 55,940 represent a significant increase in cAMP levels relative to CP 55,940 cAMP suppression, $^{*}P < 0.05$, and $^{**}P < 0.01$. Asterisks next to different tested concentrations of SMM-189 represent significant increases in the EC_{50} of CP 55,940 from base line levels, $^{*}P < 0.05$, $^{**}P < 0.01$, $^{***}P < 0.001$, $^{****}P < 0.0001$. HEK-CNG+CB1, Human embryonic kidney cells transfected with a cyclic nucleotide-gated channel and cannabinoid receptor 1; SMM-189, 3′,5′-dichloro-2,6-dihydroxy-biphenyl-4-yl)-phenyl-methanone.

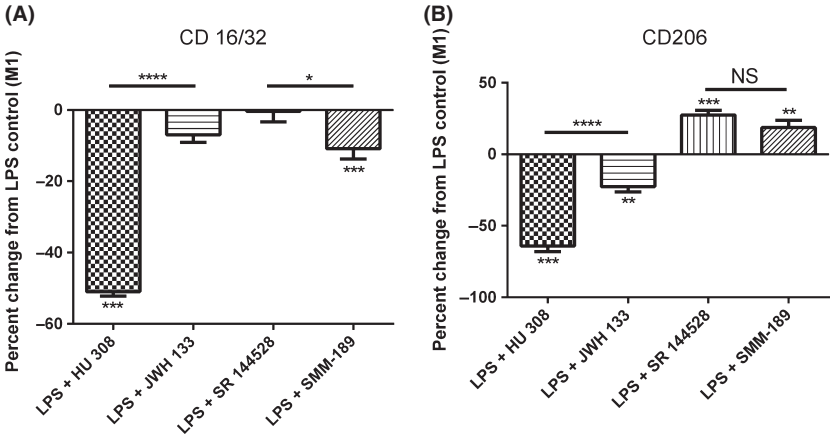

Figure 4. (A) In C8B4 murine microglia, CB2 agonists HU 308 and JWH 133 decrease M1 marker CD16/32 at 24 h, although HU 308 treatment is significantly different from LPS control ($^{***}P < 0.001$) and JWH treatment ($^{****}P < 0.0001$). CB2 inverse agonists SR 144528 and SMM-189 decrease M1 CD16/32 as well, although only SMM-189 is significantly different from LPS control ($^{***}P < 0.001$) and SR 144528 ($^{*}P < 0.05$). (B) CB2 agonists HU 308 and JWH 133 also significantly decrease M2 marker CD 206 at 24 h compared to LPS control ($^{**}P < 0.01$, $^{***}P < 0.001$) and HU 308 was decreased CD206 significantly more than JWH 133 ($^{****}P < 0.0001$). CB2 inverse agonists SR 144528 and SMM-189 increased CD206 significantly more in response to LPS controls ($^{***}P < 0.001$, $^{**}P < 0.01$) and were not significantly different from each other. $N = 3$–9, error is SEM. Asterisks above columns are comparisons to LPS control, while bar comparisons are significant in comparison to the covered columns. LPS, lipopolysaccharide; SMM-189, 3′,5′-dichloro-2,6-dihydroxy-biphenyl-4-yl)-phenyl-methanone.

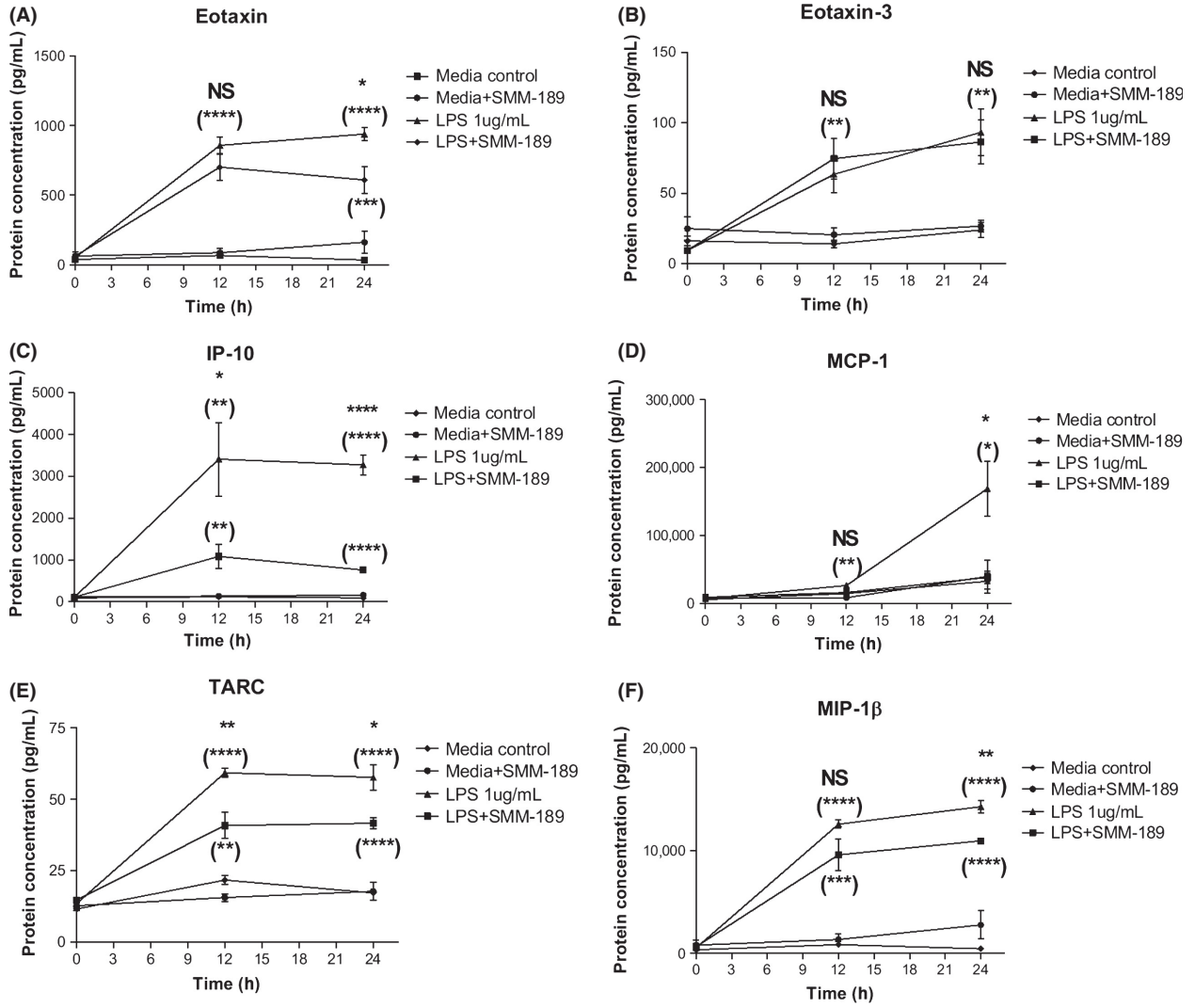

Figure 5. Time course of chemokine secretion from PHMG. $N = 4$, error bars are SD. *$P < 0.05$, **$P < 0.01$, ***$P < 0.001$, ****$P < 0.0001$. Asterisk comparisons are between LPS and LPS + SMM-189 groups, and parenthetical asterisks are comparisons of LPS or LPS + SMM-189 to media controls. Analysis done via ANOVA with Dunnett's multiple comparisons. LPS, lipopolysaccharide; PHMG, primary human microglia; SMM-189, 3′,5′-dichloro-2,6-dihydroxy-biphenyl-4-yl)-phenyl-methanone.

The LPS-treated PHMG exhibited many of the hallmarks of activated microglia including a transition to an amoeboid form or significant contraction of the cell membrane (Chen et al. 2012). At 24 h, a greater percentage of LPS-stimulated microglia had round or amoeboid morphology (Fig. 7A) ($P < 0.001$) and lower percentage of rod-shaped cells (Fig. 7B) compared to media controls. In the presence of SMM-189, media control microglia had a significantly higher percentage of rod-shaped cells with a corresponding decrease in round or amoeboid shaped cells ($P < 0.01$). In LPS-stimulated cells treated with SMM-189, there was a significant decrease in round- or amoeboid-shaped cells and increase in rod-shaped cells compared to LPS alone stimulated cells ($P < 0.001$). Media control + SMM-189 and LPS + SMM-189 groups were not significantly different from each other.

Biopharmaceutical properties of SMM-189

Aqueous solubility is one of the most important properties for a compound intended to continue into clinical studies. The solubility of SMM-189 was found to be ~185 μg/mL at pH 7.4 (Table 2). Though there is no strict cutoff value for solubility available, solubility above 50 μg/mL is arbitrarily considered acceptable for compound progression in most preclinical development programs. Despite being highly lipophilic with a clogP value of ~5.26, SMM-189 meets this benchmark, suggesting that

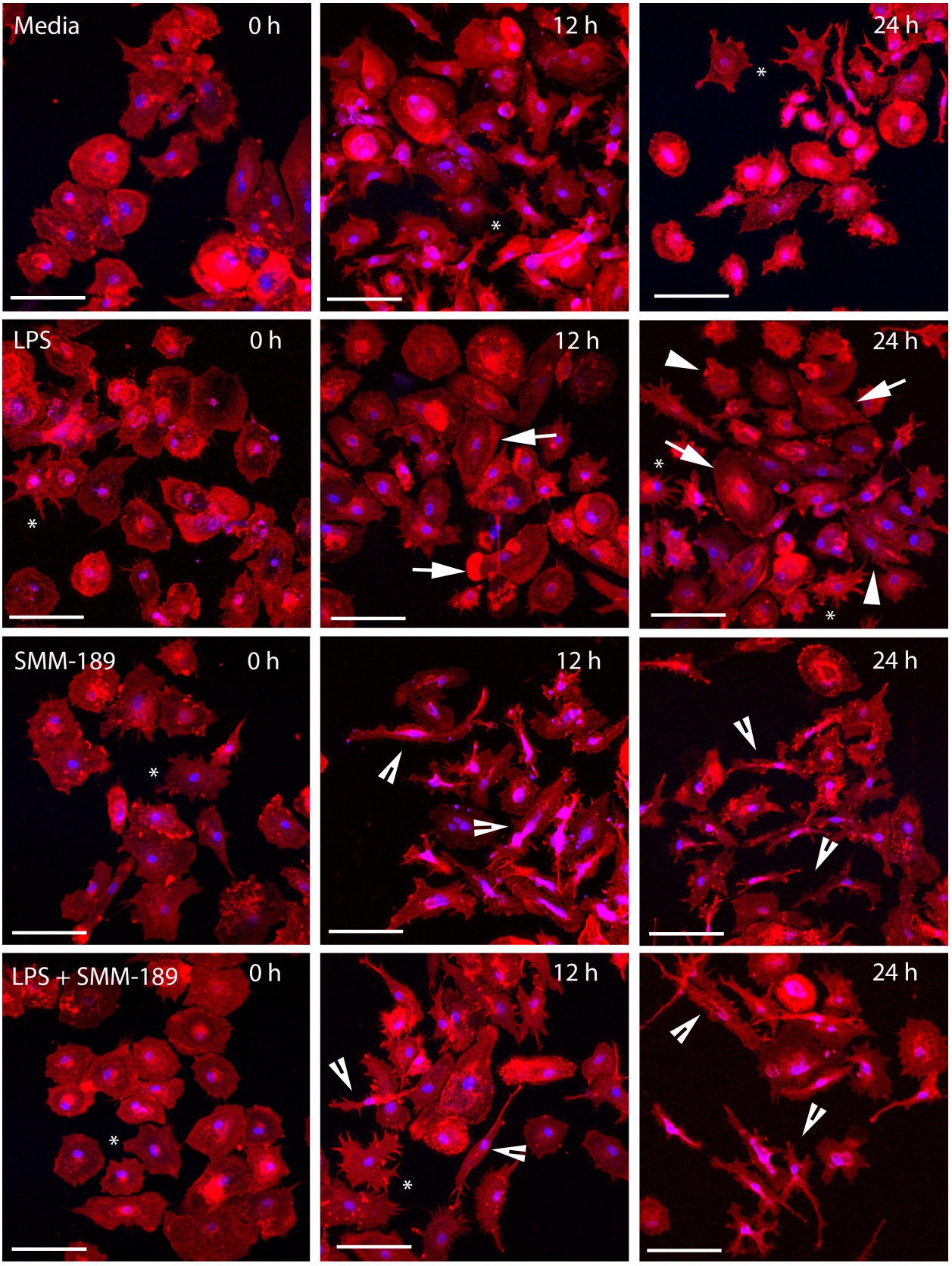

Figure 6. Representative photomicrographs of the evaluation of the actin filaments to assess PHMG cell morphology (40×). Images of PHMG cells treated with LPS, SMM-189, and LPS + SMM-189 at 0, 12, and 24 h, along with the control of PHMG cells subjected to media change. The labels appear as follows: cell nuclei with Hoechst (blue) and phalloidin-stained actin filaments (red). At 0 h, a spherical morphology with few projections is manifested in all groups. The time course of LPS treatment reveals either a progressive increase in size (white arrows) or pronounced contraction (arrow heads). The most significant difference between treatment groups is the emergence of the rod-shaped morphology associated with SMM-189 treatment alone or in the presence of LPS (chevrons). White bars in each photomicrograph represent 100 μm. LPS, lipopolysaccharide; PHMG, primary human microglia; SMM-189, 3′,5′-dichloro-2,6-dihydroxy-biphenyl-4-yl)-phenyl-methanone.

the compound might have sufficient solubility for dosage form development and at the same time a sufficiently high lipophilicity to cross biological membranes (Table 2). This observation is supported by data from a parallel artificial membrane permeability assay (PAMPA) where the permeability of SMM-189 was determined as -5.02 ± 0.02 cm/sec at pH 7.4 (Table 2).

Pharmacokinetic properties of SMM-189

To assess in vitro metabolic stability, SMM-189 was incubated in rat liver microsomal preparations. SMM-189 exhibited acceptable metabolic stability with 45.3% of the parent compound remaining stable at the end of a 90-min incubation period (Table 2). Protein-binding experiments suggest, however, that SMM-189 is highly bound to plasma proteins, with $99.37 \pm 0.01\%$ at 500 ng/mL and $99.84 \pm 0.02\%$ at 2 μg/mL. Initial data on the pharmacokinetics of SMM-189 in vivo confirm the results of the in vitro assays discussed above. Administration of a single 5 mg/kg dose by intravenous injection in rats resulted in plasma-concentration-time profiles with peak plasma concentrations of 6.23 ± 1.67 mg/L with a terminal half-life of 3.03 ± 0.49 h (Fig. 8), indicating reasonable in vivo metabolic stability. The volume of distribution was determined as 14.9 ± 2.38 L/kg, indicating extensive distribution into tissues outside the vascular space.

Discussion

The objective of our studies was to further characterize SMM-189 owing to the promise of this compound in treating murine mTBI. In the ACTOne cannabinoid receptor-transfected cell lines, SMM-189 demonstrated good binding selectivity for CB2 over CB1 receptors, as well as inverse agonist activity at CB2 receptors. In this same system, we determined that SMM-189 is a noncompetitive antagonist at the CB2 receptor against CP 55,940. Many GPCR inverse agonists have been reported to act as noncompetitive antagonists when tested against agonists (Carroll et al. 2001; Fitzsimons et al. 2004; Porter et al. 2005). However, equilibrium dynamics of the inverse agonist versus an agonist are not simply a function of receptor affinities, but also inverse agonists' preferential binding to inactive receptors, which can increase cell surface expression of the targeted receptor (Smit et al. 1996; Khilnani and Khilnani 2011).

Much of the literature surrounding CB2 modulation of inflammation focuses on agonists [for an excellent review, see (Ashton and Glass 2007)] but the beneficial effect of SMM-189 in a mTBI model had suggested that it could

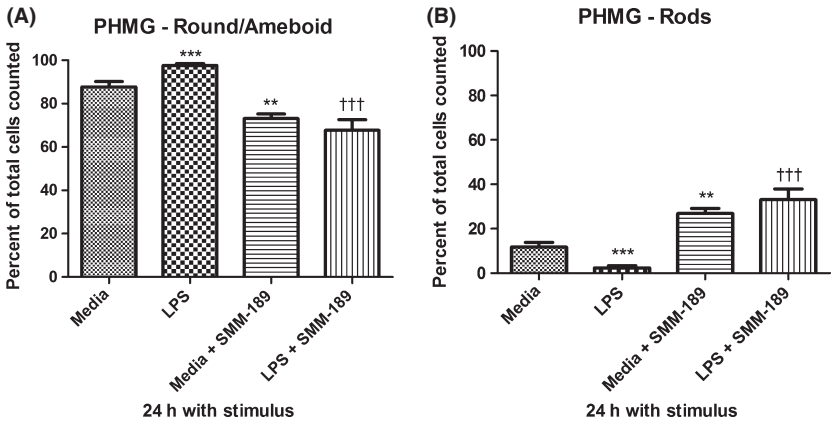

Figure 7. Percentage of (A) round/ameboid and (B) rod-shaped microglia after 24 h of control or LPS stimulus, with or without SMM-189 treatment. ANOVA analysis done with Bonferroni corrections in GraphPad Prism. $N = 4$ fields per group counted by four different researchers, error bars are SEM. LPS, lipopolysaccharide; SMM-189, 3′,5′-dichloro-2,6-dihydroxy-biphenyl-4-yl)-phenyl-methanone. $^{**}P < 0.01$, $^{***}P < 0.001$, in comparison to media control, †††p$P < 0.001$ in comparison to LPS.

Table 2. Biochemical and pharmacokinetic properties of SMM-189.

Aqueous solubility	~185 μg/mL at pH 7.4
cLogP	5.26
Membrane Permeability (log Pe)	−5.02 ± 0.02 cm/sec at pH 7.4
Microsomal stability (% of parent remaining)	45.3% at 90 min
Plasma protein binding	99.37 ± 0.01% at 500 ng/mL 99.84 ± 0.02% at 2 μg/mL
Terminal half-life	3.03 ± 0.49 h
Volume of distribution	14.9 ± 2.38 L/kg

SMM-189, 3′,5′-dichloro-2,6-dihydroxy-biphenyl-4-yl)-phenyl-methanone

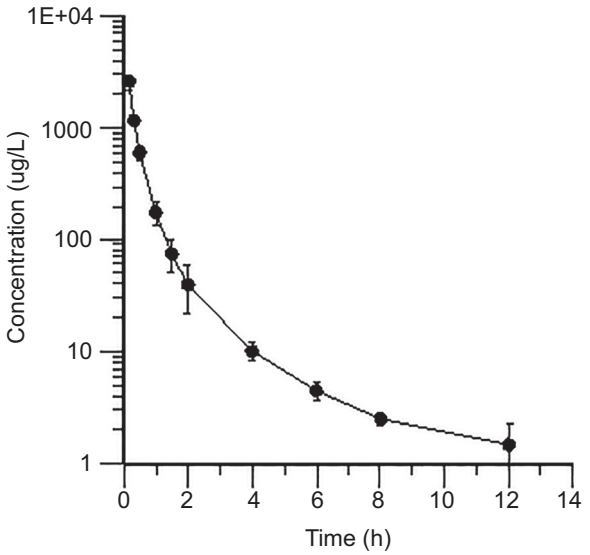

Figure 8. Mean (±SD) plasma concentration-time profiles of SMM-189 after IV administration of 5 mg/kg in rats ($N = 6$). SMM-189, 3′,5′-dichloro-2,6-dihydroxy-biphenyl-4-yl)-phenyl-methanone.

offer anti-inflammatory activities (Reiner et al. 2015). Therefore, we investigated the effects of both CB2 agonists and inverse agonists on activated, proinflammatory microglia by probing for cell surface expression of proinflammatory M1 marker, CD16/32, and pro-wound healing M2 marker, CD206. CB2 agonists HU 308 and JWH 133 decrease proinflammatory marker CD16/32, although only HU 308 treatment resulted in statistically significant decreases in CD16/32 in comparison to LPS control. While CB2 inverse agonists SR 144528 and SMM-189 decreased CD16/32 as well, but only SMM-189 did so significantly in comparison to LPS control. CD206 expression was also significantly decreased by CB2 agonists HU 308 and JWH 133, while CB2 inverse agonists SR 144528 and SMM-189 increased CD206 expression.

The results from the polarization state study suggest that CB2 agonists exert anti-inflammatory activity by decreasing both M1 and M2 markers following inflammatory stimulation. The decrease in M1 marker CD16/32 is consistent with a previous study that reflected decreases in M1 markers in Kupffer cells following JWH 133 treatment (Louvet et al. 2011). The same study did not find changes in M2 markers following JWH 133 treatment, although it is worth noting that the analysis was of mRNA which may not have reflected final protein changes compared to our study. Conversely, CB2 inverse agonists SR 144528 and SMM-189 appear to exert anti-inflammatory activity by decreasing CD16/32, an M1 marker, and increasing CD206, an M2 marker, which is associated with alternatively activated microglia in a pro-wound healing state. The impact SMM-189 has on murine microglial polarization is consistent with effects previously reported in human microglia (Reiner et al. 2015). The ability of inverse agonists to enable M2 polarization is possibly due to the induction of the CB2 inactive receptor state, removing inhibition of the cAMP generation by adenylate cyclase, thereby increasing intracellular cAMP and downstream pCREB which has been linked to mannose receptor (CD206) expression (for an excellent review see (Lawrence and Natoli 2011)). Lipopolysaccharide increased proinflammatory chemokines eotaxin, eotaxin-3, IP-10, MCP-1, TARC, and MIP-1β. Eotaxin, also known as CCL11, has been positively correlated with phosphorylated tau in a murine model of tauopathy (Garwood et al. 2010). Eotaxin-3 expression was implicated in prodromal Alzheimer's disease but has no association with symptomatic Alzheimer's or other neurodegenerative diseases (Westin et al. 2012). In APP transgenic mice, expression of APP colocalizes with IP-10 and correlates with decreased neuroprotection and increased neurodegeneration, likely due to recruitment of distal microglia and peripheral macrophages in response to high levels of inflammation (Duan et al. 2008). Additionally, IP-10 has been shown to play a role in degenerative multiple sclerosis and astrogliosis by further activating microglia and acting as a powerful chemotactic for peripheral immune cells (Tanuma et al. 2006; Zhang et al. 2014). IP-10 is also elevated in human extracellular brain fluid following TBI (Helmy et al. 2011).

Similarly, MCP-1, also called CCL2, is a powerful monocyte chemokine and has been shown to recruit and activate microglia as well as peripheral macrophages (Selenica et al. 2013). MCP-1 elevations have also been implicated as a factor in progression of Alzheimer's Disease, AIDS dementia, and TBI presumably through activating microglia and macrophages (Conant et al. 1998; Helmy et al. 2011; Westin et al. 2012; Laforte et al. 2014). In TBI patients, elevations in MCP-1 were more likely in patients that later went on to develop Alzheimer's disease (Ho et al. 2012). TARC primarily recruits activated lymphocytes, and has been investigated as a biomarker,

especially in HIV-1-induced neurodegeneration, ALS, and multiple sclerosis (Narikawa et al. 2004; Pulliam et al. 2007; Kuhle et al. 2009). Increases in MIP-1β, also known as CCL4, correlate with inflammatory viral neurodegeneration, multiple sclerosis, neuromyelitis optica, and TBI (Askovic et al. 2001; D'Aversa et al. 2004; Helmy et al. 2011; Michael et al. 2013).

The reduction in eotaxin, MCP-1, and IP-10 in LPS + SMM-189-treated microglia supports the idea that SMM-189 would likely decrease infiltration of peripheral macrophages and other immune cells. This is important since peripheral macrophages have been implicated in neurodegenerative diseases such as Alzheimer's disease, multiple sclerosis, and Parkinson's disease (Wisniewski et al. 1991; Depboylu et al. 2012; Vainchtein et al. 2014). In pathological inflammatory states, activated macrophages may enter areas of tissue damage at a time of microglial deactivation, thus restarting the cycle of inflammation and beginning a cascade that may result in chronic inflammation. The lack of effect that SMM-189 displays against eotaxin-3 is unsurprising, given that eotaxin-3 has little importance in inflammatory neurodegeneration and is primarily associated with eosinophils (Blanchard et al. 2006; Westin et al. 2012). Furthermore, SMM-189 may also have a role in treating autoimmune-associated neurodegenerative disease such as multiple sclerosis and HIV/AIDS dementia that have a robust lymphoid component, in addition to monocyte recruitment as demonstrated by its effect on TARC (Depboylu et al. 2012).

Microscopic examination of unstimulated PHMG revealed the expected primarily round phenotype and projections. Lipopolysaccharide predictably caused an increase in the amoeboid shape of microglia at both 12 and 24 h. The effect of SMM-189 in LPS-treated cells was an increase in rod-shaped cells over that of amoeboid-shaped microglia. The media + SMM-189 cells that also showed an increase in rod-shaped cells, suggesting that the effect of SMM-189 is capable of overcoming the stimulatory effect associated with LPS exposure. Rod-shaped cells have been suggested to be highly beneficial in repairing neurodegenerative areas of the CNS (Tam and Ma 2014). In agreement with this proposal, we have previously shown that SMM-189 can polarize immortalized human microglia to a beneficial, pro-wound healing state, generally referred to as an M2 state (Reiner et al. 2015). The proposed M2 morphology is further correlated by the observed decrease in CD16/32 and an increase in CD206 manifest by LPS stimulated microglia in the presence of SMM-189.

The biopharmaceutical evaluation suggests that SMM-189 has acceptable solubility (~185 μg/mL at pH 7.4) and is likely to cross-biological membranes. This is supported by our PAMPA assay wherein the log Pe for permeability was determined as -5.02 $\pm$ 0.02 cm/sec at pH 7.4. When compared with permeability standards for this assay reported by Wohnsland and Faller (Wohnsland and Faller 2001), the permeability of SMM-189 was found between the value of piroxicam (−4.9) and warfarin (−5.2) at pH 7.4, which are reported to be 90–100% absorbed in humans. The high plasma binding of 99.4–99.8% is probably due to its high lipophilicity and may lead to limited, unbound effective concentrations in the CNS. However, this class of compounds has demonstrated good blood–brain barrier permeability in PET imaging studies (Fujinaga et al. 2010), thus indicating the potential for treating CNS diseases.

The in vitro metabolic stability of SMM-189 was 45.3% of the parent compound remaining at the end of a 90-min incubation period. The desired cutoff for metabolic stability in most preclinical programs is more than 30% of parent remaining stable after 90 min of incubation (White 2000). The in vivo half-life of 3.03 $\pm$ 0.49 h is consistent with the in vitro studies indicating an acceptable metabolic stability. In total, the biopharmaceutical properties suggest that the triaryl scaffold of SMM-189 represents a unique lead for future drug development.

The currently approved cannabinoid-based therapeutics, dronabinol, or nabilone for refractory emesis and Sativex for spasticity (Herman et al. 1979; Dejesus et al. 2007; Hilliard et al. 2012), suffer from psychotropic side effects, thus limiting their use in neurodegenerative disorders. The current focus for neurodegeneration in the cannabinoid field has been primarily on cannabidiol, which itself is a CB2 inverse agonist, but lacks an established mechanism of action (Thomas et al. 2007). The unmet need for new interventions to treat CNS diseases highlights the potential of CB2-based therapeutics warranting further investigation. The ability of CB2 inverse agonists to modulate inflammatory activities together with the success of SMM-189 in mitigating deleterious somatomotor effects of mTBI led to further investigations into the biological properties of SMM-189. We believe that compounds, such as SMM-189, will be valuable not only in treating CNS diseases but also serve as unique probes for studying the signaling mechanisms associated with CB2 inverse agonist anti-inflammatory activity.

Acknowledgements

Thank you to Bret Koertge for assistance with antagonist studies and Steve Gurley for receptor binding help. Additionally, Jimmy Lu from Codex Biosolutions was instrumental in establishing the ACTOne assays. Max Fletcher, Jordan Ross, Cameron Ogg, and Mounir Bendahmane counted cells in exchange for donuts. The University of Tennessee Health Science Center (UTHSC), College of Pharmacy, and the UTHSC Neuroscience Institute provided

the stipend for Chaela Presley. Endece LLC provided funding for the ACTOne assay and the biopharmaceutical evaluation of SMM-189. This work was also funded in part by National Institutes of Health grant 1S10OD016226 (Meibohm).

Author Contributions

Presley, Abidi, Meibohm, Moore participated in the research design and wrote or contributed to the writing of the manuscript. Presley, Abidi, and Suryawanshi conducted the experiments. Suryawanshi, Meibohm, Moore contributed new reagents or analytic tools. Presley, Suryawanshi performed data analysis. Mustafa contributed to the synthesis of SMM-189.

Disclosure

None declared.

References

Ashton JC, Glass M (2007). The cannabinoid CB2 receptor as a target for inflammation-dependent neurodegeneration. Curr Neuropharmacol 5: 73–80.

Askovic S, Favara C, McAtee FJ, Portis JL (2001). Increased expression of MIP-1 alpha and MIP-1 beta mRNAs in the brain correlates spatially and temporally with the spongiform neurodegeneration induced by a murine oncornavirus. J Virol 75: 2665–2674.

Bhattacharjee H, Gurley SN, Moore BM II (2009). Design and synthesis of novel tri-aryl CB2 selective cannabinoid ligands. Bioorg Med Chem Lett 19: 1691–1693.

Blanchard C, Wang N, Stringer KF, Mishra A, Fulkerson PC, Abonia JP, et al. (2006). Eotaxin-3 and a uniquely conserved gene-expression profile in eosinophilic esophagitis. J Clin Invest 116: 536–547.

Block ML, Zecca L, Hong JS (2007). Microglia-mediated neurotoxicity: uncovering the molecular mechanisms. Nat Rev Neurosci 8: 57–69.

Bouaboula M, Poinot-Chazel C, Marchand J, Canat X, Bourrie B, Rinaldi-Carmona M, et al. (1996). Signaling pathway associated with stimulation of CB2 peripheral cannabinoid receptor. Involvement of both mitogen-activated protein kinase and induction of Krox-24 expression. Eur J Biochem 237: 704–711.

Carroll FY, Stolle A, Beart PM, Voerste A, Brabet I, Mauler F, et al. (2001). BAY36-7620: a potent non-competitive mGlu1 receptor antagonist with inverse agonist activity. Mol Pharmacol 59: 965–973.

Chen Z, Jalabi W, Shpargel KB, Farabaugh KT, Dutta R, Yin X, et al. (2012). Lipopolysaccharide-induced microglial activation and neuroprotection against experimental brain injury is independent of hematogenous TLR4. J Neurosci 32: 11706–11715.

Conant K, Garzino-Demo A, Nath A, McArthur JC, Halliday W, Power C, et al. (1998). Induction of monocyte chemoattractant protein-1 in HIV-1 Tat-stimulated astrocytes and elevation in AIDS dementia. Proc Natl Acad Sci USA 95: 3117–3121.

Crowe MS, Nass SR, Gabella KM, Kinsey SG (2014). The endocannabinoid system modulates stress, emotionality, and inflammation. Brain Behav Immun 42c: 1–5.

Croxford JL (2003). Therapeutic potential of cannabinoids in CNS disease. CNS Drugs 17: 179–202.

D'Aversa TG, Yu KO, Berman JW (2004). Expression of chemokines by human fetal microglia after treatment with the human immunodeficiency virus type 1 protein Tat. J Neurovirol 10: 86–97.

Dejesus E, Rodwick BM, Bowers D, Cohen CJ, Pearce D 2007. Use of dronabinol improves appetite and reverses weight loss in HIV/AIDS-infected patients. J Int Assoc Physicians AIDS Care (Chicago, IL: 2002) 6:95–100.

Depboylu C, Stricker S, Ghobril JP, Oertel WH, Priller J, Hoglinger GU (2012). Brain-resident microglia predominate over infiltrating myeloid cells in activation, phagocytosis and interaction with T-lymphocytes in the MPTP mouse model of Parkinson disease. Exp Neurol 238: 183–191.

Duan RS, Yang X, Chen ZG, Lu MO, Morris C, Winblad B, et al. (2008). Decreased fractalkine and increased IP-10 expression in aged brain of APP(swe) transgenic mice. Neurochem Res 33: 1085–1089.

Ebner F, Brandt C, Thiele P, Richter D, Schliesser U, Siffrin V, et al. 2013. Microglial activation milieu controls regulatory T cell responses. J Immunol (Baltimore, MD: 1950) 191:5594–5602.

Elliott MB, Tuma RF, Amenta PS, Barbe MF, Jallo JI (2011). Acute effects of a selective cannabinoid-2 receptor agonist on neuroinflammation in a model of traumatic brain injury. J Neurotrauma 28: 973–981.

Fitzsimons CP, Monczor F, Fernandez N, Shayo C, Davio C (2004). Mepyramine, a histamine H1 receptor inverse agonist, binds preferentially to a G protein-coupled form of the receptor and sequesters G protein. J Biol Chem 279: 34431–34439.

Fraga D, Raborn ES, Ferreira GA, Cabral GA (2011). Cannabinoids inhibit migration of microglial-like cells to the HIV protein Tat. J Neuroimmune Pharmacol 6: 566–577.

Friese MA, Fugger L 2007. T cells and microglia as drivers of multiple sclerosis pathology. Brain: J Neurol 130:2755–2757.

Fujinaga M, Kumata K, Yanamoto K, Kawamura K, Yamasaki T, Yui J, et al. (2010). Radiosynthesis of novel carbon-11-

labeled triaryl ligands for cannabinoid-type 2 receptor. Bioorg Med Chem Lett 20: 1565–1568.

Garwood CJ, Cooper JD, Hanger DP, Noble W (2010). Anti-inflammatory impact of minocycline in a mouse model of tauopathy. Front Psychiatry 1: 136.

Gibaldi M, Perrier D, eds. (1982). Pharmacokinetics. Marcel Dekker Inc, New York.

Glomme A, Marz J, Dressman JB (2005). Comparison of a miniaturized shake-flask solubility method with automated potentiometric acid/base titrations and calculated solubilities. J Pharm Sci 94: 1–16.

Govaerts SJ, Hermans E, Lambert DM (2004). Comparison of cannabinoid ligands affinities and efficacies in murine tissues and in transfected cells expressing human recombinant cannabinoid receptors. Eur J Pharm Sci 23: 233–243.

Helmy A, Carpenter KL, Menon DK, Pickard JD, Hutchinson PJ (2011). The cytokine response to human traumatic brain injury: temporal profiles and evidence for cerebral parenchymal production. J Cereb Blood Flow Metab 31: 658–670.

Herman TS, Einhorn LH, Jones SE, Nagy C, Chester AB, Dean JC, et al. (1979). Superiority of nabilone over prochlorperazine as an antiemetic in patients receiving cancer chemotherapy. N Engl J Med 300: 1295–1297.

Hilliard A, Stott C, Wright S, Guy G, Pryce G, Al-Izki S, et al. (2012). Evaluation of the effects of sativex (THC BDS: CBD BDS) on inhibition of spasticity in a chronic relapsing experimental allergic autoimmune encephalomyelitis: a model of multiple sclerosis. ISRN Neurol 2012: 802649.

Ho L, Zhao W, Dams-O'Connor K, Tang CY, Gordon W, Peskind ER, et al. (2012). Elevated plasma MCP-1 concentration following traumatic brain injury as a potential "predisposition" factor associated with an increased risk for subsequent development of Alzheimer's disease. J Alzheimer's Dis 31: 301–313.

Kerns EH, Di L, Petusky S, Farris M, Ley R, Jupp P (2004). Combined application of parallel artificial membrane permeability assay and Caco-2 permeability assays in drug discovery. J Pharm Sci 93: 1440–1453.

Khilnani G, Khilnani AK (2011). Inverse agonism and its therapeutic significance. Indian J Pharmacol 43: 492–501.

Kozela E, Pietr M, Juknat A, Rimmerman N, Levy R, Vogel Z (2010). Cannabinoids Delta(9)-tetrahydrocannabinol and cannabidiol differentially inhibit the lipopolysaccharide-activated NF-kappaB and interferon-beta/STAT proinflammatory pathways in BV-2 microglial cells. J Biol Chem 285: 1616–1626.

Krishnamurthy M, Gurley S, Moore BM II (2008). Exploring the substituent effects on a novel series of C1′-dimethyl-aryl Delta8-tetrahydrocannabinol analogs. Bioorg Med Chem 16: 6489–6500.

Kuhle J, Lindberg RL, Regeniter A, Mehling M, Steck AJ, Kappos L, et al. (2009). Increased levels of inflammatory chemokines in amyotrophic lateral sclerosis. Eur J Neurol 16: 771–774.

Laforte V, Marcoux J, Juncker D (2014) Time profiles of 50 proteins measured in the brain tissue, cerebrospinal fluid and blood of severe traumatic brain injury patients, in, HUPO 13th Annual World Congress.

Lawrence T, Natoli G (2011). Transcriptional regulation of macrophage polarization: enabling diversity with identity. Nat Rev Immunol 11: 750–761.

Liu B, Hong JS (2003). Role of microglia in inflammation-mediated neurodegenerative diseases: mechanisms and strategies for therapeutic intervention. J Pharmacol Exp Ther 304: 1–7.

Lively S, Schlichter LC (2013). The microglial activation state regulates migration and roles of matrix-dissolving enzymes for invasion. J Neuroinflammation 10: 75.

Lou ZY, Chen C, He Q, Zhao CB, Xiao BG (2011). Targeting CB(2) receptor as a neuroinflammatory modulator in experimental autoimmune encephalomyelitis. Mol Immunol 49: 453–461.

Louvet A, Teixeira-Clerc F, Chobert MN, Deveaux V, Pavoine C, Zimmer A, et al. 2011. Cannabinoid CB2 receptors protect against alcoholic liver disease by regulating Kupffer cell polarization in mice. Hepatology (Baltimore, MD) 54:1217–1226.

Lunn CA, Reich EP, Fine JS, Lavey B, Kozlowski JA, Hipkin RW, et al. (2008). Biology and therapeutic potential of cannabinoid CB2 receptor inverse agonists. Br J Pharmacol 153: 226–239.

Martin-Moreno AM, Reigada D, Ramirez BG, Mechoulam R, Innamorato N, Cuadrado A, et al. (2011). Cannabidiol and other cannabinoids reduce microglial activation in vitro and in vivo: relevance to Alzheimer's disease. Mol Pharmacol 79: 964–973.

Merighi S, Gessi S, Varani K, Simioni C, Fazzi D, Mirandola P, et al. (2012). Cannabinoid CB(2) receptors modulate ERK-1/2 kinase signalling and NO release in microglial cells stimulated with bacterial lipopolysaccharide. Br J Pharmacol 165: 1773–1788.

Michael BD, Elsone L, Griffiths MJ, Faragher B, Borrow R, Solomon T, et al. (2013). Post-acute serum eosinophil and neutrophil-associated cytokine/chemokine profile can distinguish between patients with neuromyelitis optica and multiple sclerosis; and identifies potential pathophysiological mechanisms - a pilot study. Cytokine 64: 90–96.

Mukhopadhyay S, Das S, Williams EA, Moore D, Jones JD, Zahm DS, et al. (2006). Lipopolysaccharide and cyclic AMP regulation of CB(2) cannabinoid receptor levels in rat brain and mouse RAW 264.7 macrophages. J Neuroimmunol 181: 82–92.

Narikawa K, Misu T, Fujihara K, Nakashima I, Sato S, Itoyama Y (2004). CSF chemokine levels in relapsing neuromyelitis optica and multiple sclerosis. J Neuroimmunol 149: 182–186.

Ortega-Gutierrez S, Molina-Holgado E, Arevalo-Martin A, Correa F, Viso A, Lopez-Rodriguez ML, et al. (2005). Activation of the endocannabinoid system as therapeutic approach in a murine model of multiple sclerosis. FASEB J 19: 1338–1340.

Porter RH, Jaeschke G, Spooren W, Ballard TM, Buttelmann B, Kolczewski S, et al. (2005). Fenobam: a clinically validated nonbenzodiazepine anxiolytic is a potent, selective, and noncompetitive mGlu5 receptor antagonist with inverse agonist activity. J Pharmacol Exp Ther 315: 711–721.

Pulliam L, Sun B, Rempel H, Martinez PM, Hoekman JD, Rao RJ, et al. (2007). Intranasal tat alters gene expression in the mouse brain. J Neuroimmune Pharmacol 2: 87–92.

Reiner A, Heldt SA, Presley CS, Guley NH, Elberger AJ, Deng Y, et al. (2015). Motor, visual and emotional deficits in mice after closed-head mild traumatic brain injury are alleviated by the novel CB2 inverse agonist SMM-189. Int J Mol Sci 16: 758–787.

Rhee MH, Kim SK (2002). SR144528 as inverse agonist of CB2 cannabinoid receptor. J Vet Sci 3: 179–184.

Ribeiro R, Wen J, Li S, Zhang Y (2013). Involvement of ERK1/2, cPLA2 and NF-kappaB in microglia suppression by cannabinoid receptor agonists and antagonists. Prostaglandins Other Lipid Mediat 100–101: 1–14.

Romero-Sandoval EA, Horvath R, Landry RP, DeLeo JA (2009). Cannabinoid receptor type 2 activation induces a microglial anti-inflammatory phenotype and reduces migration via MKP induction and ERK dephosphorylation. Mol Pain 5: 25.

Selenica ML, Alvarez JA, Nash KR, Lee DC, Cao C, Lin X, et al. (2013). Diverse activation of microglia by chemokine (C-C motif) ligand 2 overexpression in brain. J Neuroinflammation 10: 86.

Shohami E, Cohen-Yeshurun A, Magid L, Algali M, Mechoulam R (2011). Endocannabinoids and traumatic brain injury. Br J Pharmacol 163: 1402–1410.

Sipe JC, Arbour N, Gerber A, Beutler E (2005). Reduced endocannabinoid immune modulation by a common cannabinoid 2 (CB2) receptor gene polymorphism: possible risk for autoimmune disorders. J Leukoc Biol 78: 231–238.

Smit MJ, Leurs R, Alewijnse AE, Blauw J, Van Nieuw Amerongen GP, Van De Vrede Y, et al. (1996). Inverse agonism of histamine H2 antagonist accounts for upregulation of spontaneously active histamine H2 receptors. Proc Natl Acad Sci USA 93: 6802–6807.

Stella N (2010). Cannabinoid and cannabinoid-like receptors in microglia, astrocytes, and astrocytomas. Glia 58: 1017–1030.

Tam WY, Ma CH (2014). Bipolar/rod-shaped microglia are proliferating microglia with distinct M1/M2 phenotypes. Sci Rep 4: 7279.

Tanuma N, Sakuma H, Sasaki A, Matsumoto Y (2006). Chemokine expression by astrocytes plays a role in microglia/macrophage activation and subsequent neurodegeneration in secondary progressive multiple sclerosis. Acta Neuropathol 112: 195–204.

Thomas A, Baillie GL, Phillips AM, Razdan RK, Ross RA, Pertwee RG (2007). Cannabidiol displays unexpectedly high potency as an antagonist of CB1 and CB2 receptor agonists in vitro. Br J Pharmacol 150: 613–623.

Vainchtein ID, Vinet J, Brouwer N, Brendecke S, Biagini G, Biber K, et al. (2014). In acute experimental autoimmune encephalomyelitis, infiltrating macrophages are immune activated, whereas microglia remain immune suppressed. Glia 62: 1724–1735.

Walter L, Franklin A, Witting A, Wade C, Xie Y, Kunos G, et al. (2003). Nonpsychotropic cannabinoid receptors regulate microglial cell migration. J Neurosci 23: 1398–1405.

Westin K, Buchhave P, Nielsen H, Minthon L, Janciauskiene S, Hansson O (2012). CCL2 is associated with a faster rate of cognitive decline during early stages of Alzheimer's disease. PLoS ONE 7: e30525.

White RE (2000). High-throughput screening in drug metabolism and pharmacokinetic support of drug discovery. Annu Rev Pharmacol Toxicol 40: 133–157.

Wisniewski HM, Barcikowska M, Kida E (1991). Phagocytosis of beta/A4 amyloid fibrils of the neuritic neocortical plaques. Acta Neuropathol 81: 588–590.

Witkamp R, Meijerink J (2014). The endocannabinoid system: an emerging key player in inflammation. Curr Opin Clin Nutr Metab Care 17: 130–138.

Wohnsland F, Faller B (2001). High-throughput permeability pH profile and high-throughput alkane/water log P with artificial membranes. J Med Chem 44: 923–930.

Zarruk JG, Fernandez-Lopez D, Garcia-Yebenes I, Garcia-Gutierrez MS, Vivancos J, Nombela F, et al. (2012). Cannabinoid type 2 receptor activation downregulates stroke-induced classic and alternative brain macrophage/microglial activation concomitant to neuroprotection. Stroke 43: 211–219.

Zhang Y, Gao Z, Wang D, Zhang T, Sun B, Mu L, et al. (2014). Accumulation of natural killer cells in ischemic brain tissues and the chemotactic effect of IP-10. J Neuroinflammation 11: 79.

Zoppi S, Madrigal JL, Caso JR, Garcia-Gutierrez MS, Manzanares J, Leza JC, et al. (2014). Regulatory role of the cannabinoid CB2 receptor in stress-induced neuroinflammation in mice. Br J Pharmacol 171: 2814–2826.

Supporting Information

Additional Supporting Information may be found in the online version of this article:

Table S1. EC50 Comparisons Between Receptor Binding Assays.